INTERNATIONAL JOURNAL OF PRECISION ENGINEERING AND MANUFACTURING Vol. 16, No. 3, pp. 419-422 MARCH 2015 / 419
DOI: 10.1007/s12541-015-0057-6

Electrochemical Oxidation Assisted Micromachining of Glassy Carbon Substrate

Wonkyun Lee[1], Eunseok Nam[1], Chan-Young Lee[1], Kyung-In Jang[2], and Byung-Kwon Min[1,#]

1 School of Mechanical Engineering, Yonsei University, 50 Yonsei-ro, Seodaemun-gu, Seoul, 120-749, South Korea
2 Department of Materials Science and Engineering and Frederick Seitz Materials Research Laboratory, University of Illinois at Urbana-Champaign, Urbana, IL 61801, USA
Corresponding Author / E-mail: bkmin@yonsei.ac.kr, TEL: +82-2-2123-5813, FAX: +82-2-364-6769

KEYWORDS: Hybrid machining, Difficult-to-machine material, Non-traditional machining

Glassy carbon (GC) has merits to be used as mold material for glass molding press because of its superior chemical and thermal properties. However, it is difficult to machine GC mechanically because of its brittleness and hardness. Undesired fractures and cracks are frequently generated on the machined surfaces. A novel micromachining process for precision machining of GC that combines mechanical micromachining and electrochemical oxidation has been developed. In the proposed process, an oxide layer is generated on the GC surface and removed mechanically. In the contact area between the tool and workpiece, the generation and removal of the oxide layer are repeated. A number of experimental results are presented to investigate the machining characteristics and to show the feasibility of the proposed process.

Manuscript received: October 8, 2014 / Revised: November 14, 2014 / Accepted: November 23, 2014

1. Introduction

Glassy carbon (GC) is used widely as an electrode material in electrochemical devices because of its high chemical stability and gas impermeability.[1] Recently, GC was introduced as a mold material for precision glass molding processes because of its high hardness, operating temperature, and wear resistance and low thermal expansion coefficient. Furthermore, molded glass products are easily separated from the mold because of the low cohesion between the glass and GC. However, at the same time, the hardness and brittleness of GC make it difficult to machine mechanically.[2] Dicing, laser ablation, and focused ion beam have been applied for the precision machining of GC. Dicing using a diamond saw is the simplest technique to machine GC and can achieve high surface quality. Using a dicing saw, Magee and Osteryoung[3] fabricated GC linear array electrodes for use as electrochemical detectors in flow cells. Youn et al.[4] fabricated a pyramidal GC mold using a dicing saw. However, dicing cannot be used for three-dimensional (3D) machining. Laser machining has also been assessed. Using a laser, Kuhnke et al.[5] fabricated a GC electrode with high aspect ratio channels. However, direct laser ablation lacks the form accuracy because of the beam shape and the heat generated can alter the material properties. Focused ion beam milling has been used on micrometer and nanometer scales. Takahashi et al.[6] and Youn et al.[7] fabricated GC micromolds using FIB milling with nanometer-scale accuracy. However, the machining speed of FIB milling is slow and the machining area is limited to the micrometer range.

To overcome these limitations, a novel hybrid micromachining process is proposed using a combination of electrochemical oxidation of the surface and mechanical machining. A thin oxide layer is generated on the GC surface by applying overvoltage between the GC and electrolyte. This oxide layer is easily removed by mechanical machining because its hardness is lower than that of GC. Simultaneously, the oxide layer is regenerated on the surface exposed to the electrolyte. At the contact area between the material and machine tool, the generation and removal of the oxide layer on the material is repeated.

An experimental machine tool with three axes was built in which the workpiece was located in an electrochemical cell. A series of experiments was performed to verify the feasibility of the proposed process and investigate the machining characteristics. A Tafel experiment was performed to identify the electrochemical behavior of GC and to obtain the ideal overvoltage for machining. A line pattern was fabricated to demonstrate that the proposed process generated a high-quality surface.

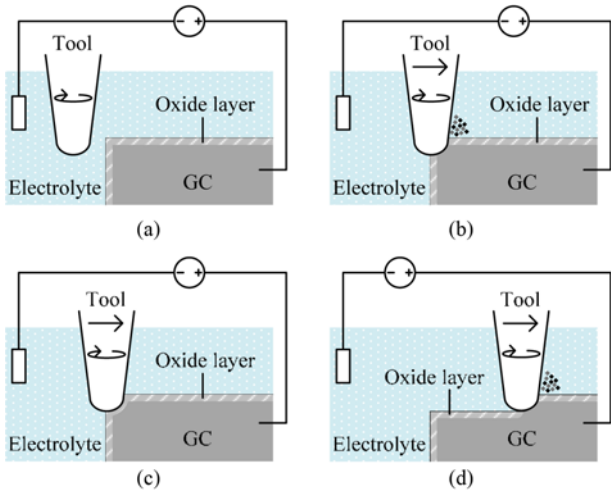

Fig. 1 Electrochemical oxidation assisted micromachining processes: (a) formation of oxide layer before machining, (b) removal of GC substrate with its oxide layer, (c) regeneration of oxide layer and (d) machining of GC workpiece by the repetition of the (b) and (c)

2. Electrochemical Oxidation Assisted Micromachining

2.1 Machining process

Fig. 1 shows a schematic of the machining processes. (a) The overvoltage between the GC and electrolyte causes active polarization. As a result, a thin oxide layer (< 5 nm) is generated on the GC surface.[8] (b) When the machining starts, the GC substrate with its oxide layer is removed mechanically. (c) Simultaneously, the oxide layer is regenerated on the newly exposed fresh GC surface. (d) The GC is machined by the repeating steps (b) and (c).

In the proposed machining process the oxide layer is generated continuously on the machined surface and removed easily because the hardness of the oxide layer is lower than GC substrate.[9] This synergetic effect increases the material removal rate without crack propagation although the thickness of the generated oxide layer is very thin.

2.2 Electrochemical behavior of GC

A variety of electrochemical reactions occur on the GC surface depending on the overvoltage applied. The electrochemical behavior of GC (relationship between the overvoltage and reaction) was tested using Tafel experiments. A precision potentiostat (PARSTAT 2273, Princeton Applied Research) was used to supply the overvoltage and to monitor the current. In this study, 1 M NaOH was used as the electrolyte for electrochemical oxidation. A platinum wire counter electrode (ALS) and Hg/HgO reference electrode (CHI) were used for the Tafel experiment. Fig. 2 plots the polarization curve for voltages from –0.25 to 2.25 V *vs*. a standard hydrogen electrode (SHE). The open circuit voltage (OCV) of GC was measured as –14 mV *vs*. SHE.

A cathodic reaction occurred on the GC sample surface in the region under the OCV. The overvoltage above the OCV could be divided into four regions according to the applied overvoltage. In Region 1 (OCV ~ 0.76 V) of the graph, the current density increases uniformly as a result of the ionization of carbon atoms on the GC surface as

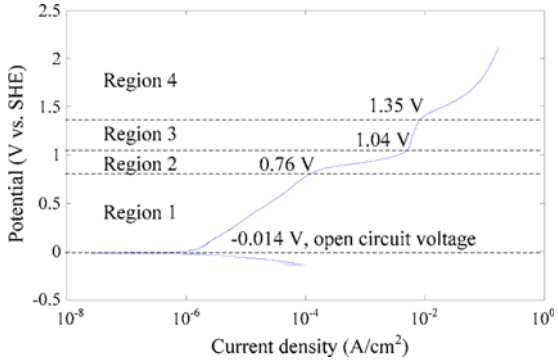

Fig. 2 Polarization curve of GC derived from the Tafel experiment

$$C \rightarrow C^{+} + e^{-} \tag{1}$$

When the overvoltage reaches Region 2 (0.76~1.04 V), an oxide layer starts to be generated on the GC surface via the following reactions:

$$C^{+} + H_2O \rightarrow C-OH + H^{+} \tag{2}$$

$$C-OH \rightarrow C=O + H^{+} + e^{-} \tag{3}$$

The slope of the Tafel curve decreases because the number of electrons involved in the reaction increases. Material loss is increased in this region as a result of the synergism between mechanical machining and the electrochemical reaction.

In Region 3 (1.04~1.35 V), the oxide layer on the GC surface starts to be dissolved. Both passivation and dissolution reactions are occurred simultaneously.[10] However, the material removal caused by the dissolution of the oxide layer is ignorable in this region because the dissolution rate is small.

If the overvoltage reaches Region 4 (> 1.35 V), the dominant reaction between the GC and electrolyte is electrolysis of the electrolyte. Hydrogen and oxygen gases are generated on the counter electrode and workpiece, respectively. In this region, the material loss caused by dissolution constitutes a great part of the total material loss.

3. Experimental

3.1 Experimental setup

Fig. 3 is a schematic of the machine tool setup. Two linear stages (VP25-XA, Newport) were used as the *x*- and *y*-axes. A linear stage (ILS250-CCHA, Newport) with an axial load capacity of 40 N was used as the *z*-axis. Linear scales with a resolution of 0.1 m were used to measure the position. A pulley spindle (NSK 302P, Nakanishi) was connected to a servomotor with a maximum speed of 3,000 RPM. A tool dynamometer (9256C1, Kistler) with a sensitivity of –26 pC/N was used to measure the normal force during machining. An electrochemical cell was installed on the tool dynamometer. The machine tool was controlled by using a real-time computer (DS1103, dSPACE).

When selecting the tool material, the ionization tendency of the material must be lower than that of GC. If the ionization tendency

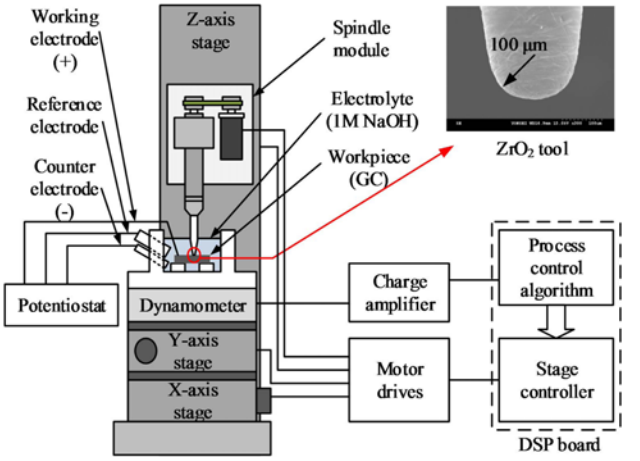

Fig. 3 Schematic view of the machine tool setup

exceeds that of GC the more electrochemical reaction occurs at the tool surface and an oxide layer is generated on the tool surface instead of the GC surface. The hardness of the tool must exceed that of GC to avoid tool failure during machining. To meet these requirements, a specially designed zirconia (ZrO_2) tool was used for machining. The electron micrograph in Fig. 3 shows the shape of the zirconia tool after machining.

During machining, the crack propagation in GC depends on the stress field.[11,12] Therefore, the machining stress applied to the GC surface must be maintained lower than the fracture stress to produce a fracture-free surface. However, it is difficult to measure the machining stress of GC because the oxide layer is removed simultaneously. In this regard, the critical normal load must be determined experimentally. The normal load applied on the GC is measured with a tool dynamometer and kept under the reference value by controlling the z-axis position. The horizontal feed rate and spindle speed are maintained constantly.

3.2 Synergetic effect on material removal

To investigate the material loss caused by the synergism between mechanical machining and electrochemical reaction line machining, results with a variety of applied overvoltages were compared. The overvoltage was applied in the middle of line machining, where the normal load and horizontal feed rate were maintained at 2 N and 0.01 mm/s, respectively. Fig. 4 shows a cross-sectional measure using a white light interferometer (NV6300, Zygo) and the overvoltage conditions. As can be seen, the machining depth was increased in the region where the overvoltage was applied.

Fig. 5 shows the relationship between the applied overvoltage and the synergetic effect. The ratio between the cross-sectional area of the regions without (S_0) and with (S) the overvoltage was compared. Line machining was performed five times for each condition. The figure supports the result of the Tafel experiment, as described in Fig. 2. The synergetic effect is turned up when the applied overvoltage exceeds that of Region 1, and increases until the overvoltage reaches 1.2 V.

The synergetic effect is maximized at 1.2 V, even in Region 3, because of the material removal by dissolution is negligible as mentioned in Section 2. The synergetic effect is reduced because the growth of the passivation rate is smaller than that of the dissolution

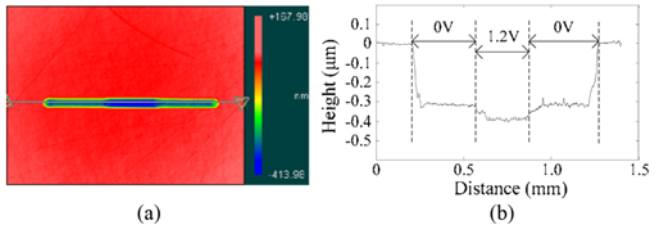

Fig. 4 Line machining result: (a) white light interferometer image and (b) depth profile with the overvoltage condition

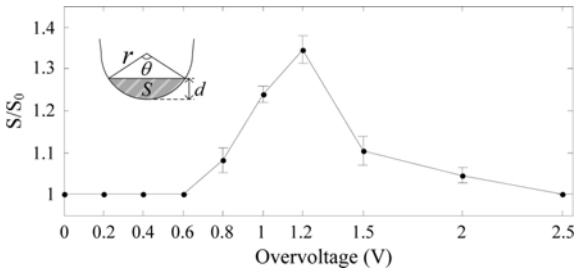

Fig. 5 Relationship between the applied overvoltage and the synergetic effect ($S = 0.5(\theta - \sin\theta)r^2$)

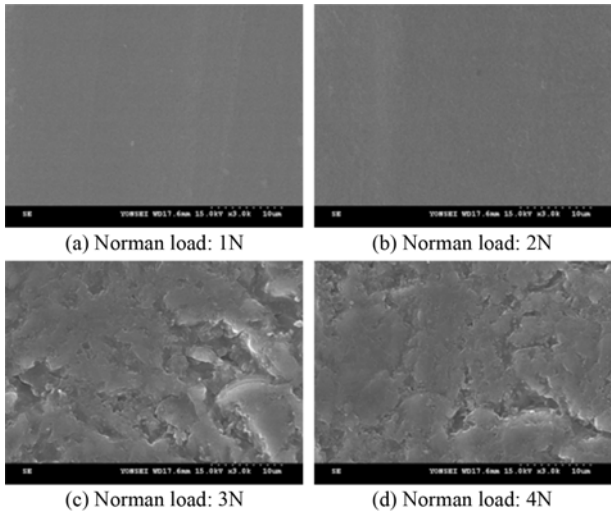

Fig. 6 Machined surface when a variety of normal load was applied

rate. The effect is disappeared at the overvoltage of 2.5 V at which the dissolution rate passes the passivation rate. Therefore, overvoltage of 1.2 V has been applied for the proposed machining.

3.3 Critical normal load for fracture-free machining

To identify the critical normal load for fracture-free machining, the machining results with normal loads from 1 to 4 N in 1-N steps were compared using an overvoltage of 1 V. The horizontal axis feed rate was maintained at 0.01 mm/s. Fig. 6 shows an electron microscopy image of the machined surface. Cracks remained on the machined surface when the reference normal load exceeded 3 N. Therefore, the critical value of the normal load for fracture-free machining is 2-3 N.

Table 1 Machining conditions for electrochemical oxidation assisted micromachining

Conditions	Description
Workpiece	GC
Electrolyte	1M NaOH
Reference electrode	Hg / HgO
Counter electrode	Pt
Tool radius	0.1 mm (ZrO_2)
Overvoltage	1.2 V
Rotation frequency	3000 RPM
Normal load (reference)	2 N
Horizontal feedrate	0.01 mm/s

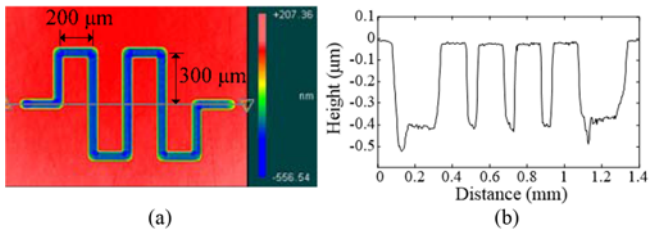

Fig. 7 Line pattern machining result: (a) white light interferometer image and (b) depth profile

Based on the results, the normal load was maintained under 2 N during machining. A line pattern with a travel length of 3.6 mm and a depth of 400 nm could be fabricated without cracks on the surface using the machining conditions listed in Table 1. Fig. 7 shows the white light interferometer (WLI) image and depth profile of the machining result.

4. Conclusions

Electrochemical oxidation assisted mechanical micromachining GC substrates has been proposed. From the series of experiments, machining conditions such as the overvoltage and reference normal load were investigated. A line pattern was fabricated to verify that the proposed method could be used for high-quality surface generation, as well as the flexibility of multi-axis machining.

ACKNOWLEDGEMENT

This work was supported by the National Research Foundation of Korea (NRF) grant funded by the Korean Government (MEST) (No. 2011-0018086)

REFERENCES

1. Nagaoka, T. and Yoshino, T., "Surface Properties of Electrochemically Retreated Glassy Carbon," Analytical Chemistry, Vol. 58, No. 6, pp. 1037-1042, 1986.
2. Cao, X. D., Kim, B. H., and Chu, C. N., "Hybrid Micromachining of Glass using ECDM and Micro Grinding," Int. J. Precis. Eng. Manuf., Vol. 14, No. 1, pp. 5-10, 2013.
3. Magee, L. J. and Osteryoung, J., "Fabrication and Characterization of Glassy Carbon Linear Array Electrodes," Analytical Chemistry, Vol. 61, No. 18, pp. 2124-2126, 1989.
4. Youn, S. W., Takahashi, M., Goto, H., and Maeda. R., "Fabrication of Micro-Mold for Glass Embossing using Focused Ion Beam, Femto-Second Laser, Eximer Laser and Dicing Techniques," Journal of Materials Processing Technology, Vols. 187-188, pp. 326-330, 2007.
5. Kuhnke, M., Lippert, T., Ortelli, E., Scherer, G. G., and Wokaun, A., "Microstructuring of Glassy Carbon: Comparison of Laser Machining and Reactive Ion Etching," Thin Solid Films, Vols. 453-454, pp. 36-41, 2004.
6. Takahashi, M., Sugimoto, K., and Maeda. R., "Nanoimprint of Glass Materials with Glassy Carbon Molds Fabricated by Focused-Ion-Beam Etching," Japanese Journal of Applied Physics, Vol. 44, No. 7S, pp. 5600–5605, 2005.
7. Youn, S. W., Takahashi, M, Goto, H., and Maeda, R., "A Study on Focused Ion Beam Milling of Glassy Carbon Molds for the Thermal Imprinting of Quartz and Borosilicate Glasses," Journal of Micromechanics and Microengineering, Vol. 16, No. 12, pp. 2576-2584, 2006.
8. Jang, K.-I., Seok, J., Min, B.-K., and Lee, S. J., "An Electrochemomechanical Polishing Process Using Magnetorheological Fluid," International Journal of Machine Tools and Manufacture, Vol. 50, No. 10, pp. 869-881, 2010.
9. Jang, K.-I., Nam, E., Lee, C.-Y., Seok, J., and Min, B.-K., "Mechanism of Synergetic Material Removal by Electrochemomechanical Magnetorheological Polishing," International Journal of Machine Tools and Manufacture, Vol. 70, pp. 88-92, 2013.
10. Macdonald, D. D., "The Point Defect Model for the Passive State," Journal of the Electrochemical Society, Vol. 139, No. 12, pp. 3434-3449, 1992.
11. Ritchie, R. O., Dauskardt, R. H., Yu, W., and Brendzel, A. M., "Cyclic Fatigue-Crack Propagation, Stress-Corrosion, and Fracture-Toughness Behavior in Pyrolytic Carbon-Coated Graphite for Prosthetic Heart Valve Applications," Journal of Biomedical Materials Research, Vol. 24, No. 2, pp. 189-206, 1990.
12. Lee, S. H., Lee, K. H., Lee, S. B. and Kim, B. M., "Study of Edge-Cracking Characteristics during Thin-Foil Rolling of Cu-Fe-P Strip," Int. J. Precis. Eng. Manuf., Vol. 14, No. 12, pp. 2109-2118, 2013.